Numerical simulation and experiment of grain motion in the conveying system of ratooning rice harvesting machine

Weijian Liu[1,2], Xiwen Luo[1,2], Shan Zeng[1,2*], Ying Zang[1,2], Zhiqiang Wen[1,2], Li Zeng[1,2], Wei Gu[3]

(1. *College of Engineering, South China Agricultural University, Guangzhou 510642, China*;
2. *Key Laboratory of Key Technology on Agricultural Machine and Equipment, Ministry of Education, South China Agricultural University, Guangzhou 510642, China*;
3. *Thinker Agricultural Machinery Co., Ltd, Huzhou 313017, Zhejiang, China*)

Abstract: The mixtures, grains, and residues in the ratooning rice harvesting machine need to be conveyed forward, backward, upward, and downward. Due to such operations, often accumulation and blockage take place at the intersection of a horizontal-vertical screw conveyor, resulting in low efficiency, high power consumption, and even grain damage. In this study, a CFD-DEM approach was applied to address the above problems. Firstly, a pneumatic conveying device was designed for ratooning rice, and then the motion of the rice grains and airflow field was analyzed in detail. The effects of different cross-sectional heights and lengths of the contraction section related to the mixing cavity were examined. Finally, the three-factor quadratic regression orthogonal rotational combination method was adopted in the experiment, and the fan velocity, filling coefficient, and speed of the horizontal screw conveyor were taken as test factors. The results showed that with the increasing cross-sectional height of the contraction section in the mixing cavity, the grain velocity decreased and the dispersity increased. With increasing length of the contraction section in the mixing cavity, the area of the high-speed airflow zone increased and the diffusion effect was enhanced. At the fan velocity of 2700 r/min, the filling coefficient was 0.41, the speed of the horizontal screw conveyor was 1173 r/min, and the outlet flow optimization index was the highest, which was 45.9% higher than that obtained without airflow.

Keywords: ratooning rice, screw conveyor, grain motion, harvesting machine, CFD-DEM
DOI: 10.25165/j.ijabe.20221504.6681

Citation: Liu W J, Luo X W, Zeng S, Zang Y, Wen Z Q, Zeng L, et al. Numerical simulation and experiment of grain motion in the conveying system of ratooning rice harvesting machine. Int J Agric & Biol Eng, 2022; 15(4): 103–115.

1 Introduction

Rice is an important staple food crop in the world, whose harvesting is an important issue in its production line[1]. Because of the advantages of low cost and high benefit of ratooning rice, its plantation area is increasing year by year. With the large-scale application of ratooning rice harvesters, users also have increasing requirements for functions, especially for the velocity and convenience of grain unloading. It is estimated that when combined rice and wheat harvesting machine is engaged for grain unloading also, only the grain unloading consumes more than half of the entire harvesting time, which seriously affects the operational efficiency of the machine.

In the harvesting process, rice panicles are collected in such a way that 1/3 of the plant and root system are left for tiller growth again. At the first harvest of rice, it is necessary to ensure plant activity and soil moisture, otherwise, the ratooning buds will die and seriously affect the yield of ratooning rice. Therefore, the rice field is not exposed to the sun before rice harvest. Based on the above conditions, the ratooning rice grains have high water content, often causing blockage to the grain unloading device. The helical flow conveying is a conveying method composed of straight axial flow and eddy. In the conveying process, the axial straight flow undertakes axial conveying, which directly affects the conveying velocity of the ratooning rice. The eddy exerts a "spinning and floating" effect on the ratooning rice, which effectively reduces the accumulation of ratooning rice. With the rotation of the screw conveyor during operation, the ratooning rice grains are subjected to normal thrust and tangential friction force exerted by helical blades[2], as well as axial and circumferential friction forces exerted by the screw shaft and the side wall[3]. After the ratooning rice grains are conveyed to the junction of the horizontal and vertical conveying pipes, the vertical conveying pipe cannot send them from the junction in time, and the grains are compacted also. Consequently, the fluidity becomes poor, and a large number of grains are piled at the junction, which makes the rotation of the screw conveyor complex and sharply decreases the work efficiency. Therefore, it becomes very necessary to optimize the structure of the grain unloading device of the combined harvester.

In recent years, the CFD-DEM approach has been widely applied as an effective tool to study various particle-fluid systems[4-11]. Pneumatic conveying is usually used for the transportation of agricultural materials, and there is no research on pneumatic conveying to solve the blockage of conveying system.

Received date: 2021-04-14 **Accepted date:** 2022-03-22
Biographies: Weijian Liu, PhD candidate, research interest: agricultural mechanization, Email: 531964726@qq.com; **Xiwen Luo**, Professor, research interest: agricultural mechanization, agricultural machinery navigation, agricultural aviation, precision agriculture and intelligent agricultural equipment, Email: xwluo@scau.edu.cn; **Ying Zang**, Professor, research interest: agricultural mechanization, Email: yingzang@scau.edu.cn; **Zhiqiang Wen**, MS candidate, research interests: agricultural mechanization, Email: cm25032@163.com; **Li Zeng**, MS candidate, research interest: agricultural mechanization, Email: 577981148@qq.com; **Wei Gu**, Senior Engineer, research interest: agricultural mechanization, Email: xgnjgw@163.com.
***Corresponding author: Shan Zeng**, PhD, Associate Professor, research interest: agricultural mechanization and automation. College of Engineering, South China Agricultural University, Guangzhou 510642, China. Email: shanzeng@scau.edu.cn.

In this study, based on the characteristics of the screw conveyor of the combined harvester, a CFD-DEM approach was applied to numerically analyze and improve the junction which easily gets blocked. The result showed that the fluidity of the ratooning rice grains was enhanced, the outlet flow was increased, and the damage rate of grains was reduced.

2 Structure and working principle

2.1 Structure of the conveying device

The grain unloading and conveying device of the ratooning rice combine harvester designed in this study is mainly composed of the mixing cavity, horizontal screw conveyor, horizontal screw conveyor shell, vertical conveying pipe, and airflow device, as shown in Figure 1. The airflow device consists of a frequency conversion fan, reducer pipe, and air pipe. The airflow velocity can be adjusted by changing velocity of the frequency conversion fan. The mixing cavity is located on the left side of the horizontal screw conveyor and below the vertical conveying pipe. The frequency conversion fan is connected with the airflow inlet, below the mixing cavity, through the air pipe and reducer pipe.

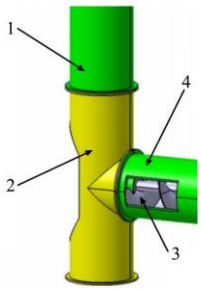

1. Vertical conveying pipe 2. Mixing cavity 3. Horizontal screw conveyor
4. Horizontal screw conveyor shell

Figure 1 Structural diagram of ratooning rice pneumatic conveying device

2.2 Working principle

During operation, the horizontal screw conveyor keeps conveying ratooning rice grains into the mixing cavity, and the high-speed airflow generated by the frequency conversion fan enters the mixing cavity through the air pipe. Then, the flow of the ratooning rice grain enters the mixing cavity and forms a gas-grain mixed flow after colliding with the high-speed airflow. Upon contact, the ratooning rice grains get dispersed due to the shearing action of the high-speed dynamic airflow and then conveyed to the upper vertical conveying pipe. The structure of the mixing cavity is shown in Figure 2.

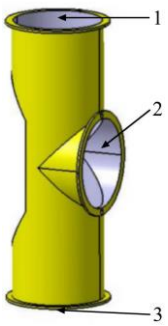

1. Gas-fluid mixed flow outlet 2. Ratooning rice grain inlet 3. Airflow inlet

Figure 2 Schematic diagram of the mixing cavity

When the airflow flows through the contraction section, its speed increases rapidly and pressure decreases to a negative value. Then, under the suction and driving effect of the horizontal screw conveyor, the ratooning rice grains enter quickly into the mixing cavity. Afterwards, the gas-grain mixed flow leaves the contraction section. As a result, the space increases and the pressure decreases. It first produces a suction effect due to the pressure difference and then realizes the diffusion effect, which makes the ratooning rice grains enter smoothly into the upper portion of the vertical conveying pipe.

3 Design of key components and determination of parameters

3.1 Parameters of ratooning rice grains

For the ratooning rice grains used in the experiments, the water content was 16%-30% and the range of density was 983-1369 kg/m^3 (approximately they were in an ellipsoid shape)[12,13]. The approximated geometric shape of a rice grain was as follows: the length of 9.00-9.35 mm, the width of 1.91-2.25 mm, the height of 4.0-6.0 mm, and the average length of 9.2 mm. Other parameters of the rationing of rice grains are listed in Table 1.

Table 1 Characteristic parameters of ratooning rice grains

Parameter	Value
Semi-axes (B×W×H)/mm	9.18×2.15×9.21
Poisson's ratio	0.25
Elastic modulus/Pa	3.75×10^8
Density/kg·m^{-3}	1330
Recovery coefficient among ratooning rice grains	0.6
Static friction factor among ratooning rice grains	0.3
Rolling friction factor among ratooning rice grains	0.01

3.2 Design of screw conveyor

The main parameters of the screw conveyor include the outer diameter of the helical blade, diameter of the central shaft, clearance distance of the helical blade from the pipe wall, helical angle at the mean radius of the blade, helical angle at the inner diameter, and pitch of the helical blade. The structure of the screw conveyor is shown in Figure 3.

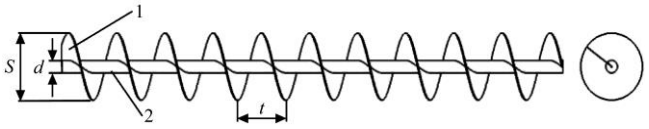

1. Helical blade 2. Central shaft

Note: S is the outer diameter of the helical blade; d is the diameter of the central shaft, and t is the pitch of the helical blade.

Figure 3 Structure of the screw conveyor

3.2.1 Outer diameter of the helical blade

The outer diameter S of the helical blade is an important index to measure the conveying capacity of the screw conveyor. In this study, S=160 mm was considered in accordance with the Agricultural Machinery Design Manual[14].

3.2.2 Diameter of the central shaft

According to the formulation of the central shaft of the screw conveyor, its diameter d can be calculated as follows:

$$d=(0.2-0.35)S \quad (1)$$

where, d is the diameter of the central shaft, mm; S is the outer diameter of the helical blade, mm.

If the diameter d of the central shaft is too large, the conveying space of the ratooning rice would become small, the ratooning rice grains would be greatly compacted, the fluidity would become poor, and the friction with the shell would increase to result in a large resistance, which would slow down the productivity and increase the energy consumption. If d is too small, the strength would be too low to meet the testing requirements. In this test, d=30 mm was taken after comprehensive consideration.

3.2.3 Pitch of the helical blade

According to the formulation of the pitch and pushing the speed of the helical blade[15], its pitch t can be obtained as follows:

$$t=(0.5-2.2)S \tag{2}$$

$$V=\frac{nt}{60} \tag{3}$$

where, t is the pitch of the helical blade, mm; n is the speed of the helical blade, r/min; V is the pushing speed of the helical blade, m/s.

The volume of the rationing rice grains is affected by the pitch t. The larger the volume of the rice, the greater the pressure on the helical blade and sidewall. With increasing t, the conveying space of the ratooning rice would increase, the ratooning rice grains would be loosely distributed with good fluidity, and the pushing speed of the ratooning rice grains would increase to result in high productivity, but the energy consumption would increase due to the increased kinetic energy of the ratooning rice grains. In this test, t=125 mm was taken after comprehensive consideration.

3.2.4 Clearance distance and helical angles at inner diameter and mean radius of the blade

The clearance between the screw conveyor and side wall is generally 5-8 mm, which was taken as 8 mm in this study. The radii at different points on the same line segment of the helical blade are different, and hence the helical angle of each point is different. The helical angle is minimum at the outer diameter and maximum at the inner diameter. The larger the helical angle is, the higher the lifting speed is, and lifting is even unavailable when the helical angle is too small[16]. In order to ensure smooth conveying of ratooning rice grains, the helical angle α_r at the inner diameter of the conveyor and the helical angle α_g at the mean radius of the conveyor blades should meet the following requirements:

$$\begin{aligned}\alpha_{\mathrm{r}} &\le 90°-\phi\\ \alpha_{\mathrm{g}} &\approx 45°-\frac{\phi}{2}\end{aligned} \tag{4}$$

where, ϕ is the friction angle between the ratooning rice and steel plate, which was taken as 25 °in this study.

3.3 Design of the airflow device

The airflow device is composed of the frequency conversion fan, reducer pipe, and air pipe. The suspension velocity of agricultural materials was the basis for the design of the pneumatic conveying system, which is an important basis for setting up a reasonable conveying speed[17-19]. Under ideal conditions, when ratooning rice grains are in the airflow field, they are acted upon by the buoyant weight ω and air force R, which can be expressed as follows:

$$\omega=\frac{\pi}{6}d_s^{\,3}(\rho_s-\rho)g \tag{5}$$

$$R=C_d\frac{\pi}{4}d_s^{\,2}\rho\frac{v_0^{\,2}}{2} \tag{6}$$

The rationing rice grains tend to move downward when $\omega>R$, while they tend to rise when $\omega<R$.

According to the mechanical formula of buoyant weight and air resistance of ratooning rice grains in the suspension state, the following relation holds:

$$C\frac{\pi}{4}d_s^{\,2}\rho\frac{v_0^{\,2}}{2}=\frac{\pi}{6}d_s^{\,3}(\rho_s-\rho)g \tag{7}$$

The suspension velocity of ratooning rice grains can be expressed as follows:

$$v_0=\sqrt{\frac{4g}{3}\frac{d_s(\rho_s-\rho)}{C\rho}} \tag{8}$$

where, v_0 is the suspension velocity of ratooning rice grains, m/s; d_s is the equivalent diameter of ratooning rice grains, m; ρ_s is the density of ratooning rice grains, kg/m^3; ρ is the air density, kg/m^3; C_d is the resistance coefficient; C is the resistance coefficient; g is the acceleration due to gravity, 9.81 m/s^2.

The results showed that the suspension velocity of ratooning rice grains was 11 m/s. Compared with the actual harvesting of ratooning rice, it was found that the humidity was high during operation, and the minimum airflow velocity had to be 15 m/s. After entering the mixing cavity, the ratooning rice grains collided with the wall surface under the action of airflow. However, the collision time was short and the force was small. Hence, the deformation of the ratooning rice grains could be ignored. The forces acting on the ratooning rice grains in the airflow field of the mixing cavity included the gravity and buoyancy, the contact force between grains, and the force between the grains and the airflow (air resistance, lift force)[20]. Hence, the following relationship was developed:

$$m_p\frac{\mathrm{d}v_p}{\mathrm{d}t}=F_D+F_{GB}+F_{Sa}+F_{Ma}+F_C \tag{9}$$

where, m_p is the mass of ratooning rice grains, kg; F_D is the fluid resistance, N; F_{GB} is the resultant force due to gravity and buoyancy, N; F_{Sa} is the Saffman lift force, N; F_C is the collision contact force between grain and wall, N; v_p is the grain velocity, m/s.

The contact force between the grains and wall surface can be expressed as follows:

$$F_C=F_{\mathrm{n}}^{\,\mathrm{d}}+F_{\mathrm{t}}^{\,\mathrm{d}} \tag{10}$$

where, $F_n^{\,d}$ is the damping force between ratooning rice grain and wall, N; $F_t^{\,d}$ is the tangential damping force, N.

$$F_n^{\,d}=-2\sqrt{\frac{5}{6}}\frac{\ln e}{\sqrt{\ln^2 e+\pi^2}}\sqrt{S_n m^*}\cdot v_n \tag{11}$$

$$F_t^{\,d}=-2\sqrt{\frac{5}{6}}\frac{\ln e}{\sqrt{\ln^2 e+\pi^2}}\sqrt{S_t m^*}\cdot v_t \tag{12}$$

where, m^* is equivalent mass; e is collision recovery coefficient; S_n is normal stiffness; S_t is tangential stiffness; v_n is the normal component of the relative velocity at the contact point; v_t is the tangential component of the relative velocity at the contact point.

3.4 Design of the mixing cavity

As the core component of the entire conveying device, the design of the mixing cavity directly affected the working efficiency of the conveying device. As shown in Figure 2 and Figure 4, the mixing cavity with a sharp and narrow middle section could produce the Venturi effect and accelerate the conveying of ratooning rice grains. The principle of the Venturi effect is that when the airflow is restricted, the velocity and pressure of the air get changed with the area of the cross section perpendicular to the airflow. When the area of the cross section is reduced, the air flow rate increases, causing a drop in the air pressure, thereby generating a negative pressure at the throat section to create an adsorption effect there. The cross-sectional height h of the contraction section should be less than the diameter D of the airflow inlet below the mixing cavity and the gas-solid mixed outlet above the mixing cavity. The diameter D=180 mm was considered, and hence the height h was within the range of 90-150 mm.

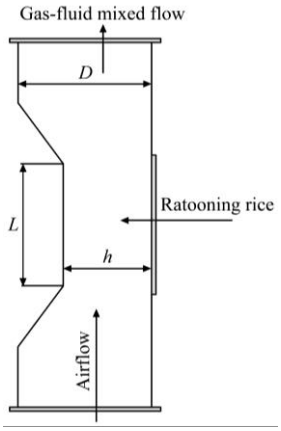

Figure 4 Schematic diagram of the mixing cavity

The pressure and velocity of air in the mixing cavity had an important influence on the flow rate of the conveying device, which was determined in terms of the cross-sectional height h and length L of the contraction section, and the air velocity v at the inlet.

4 Modeling

The discrete element method (DEM) and computational fluid dynamics (CFD) have been widely used in agricultural engineering in recent years. In the conveying device, ratooning rice grains entered the mixing cavity in the form of grain bodies, where they were mixed up with the high-speed airflow in the upward direction and then blown to the vertical conveying pipe at a certain velocity. The structure of the mixing cavity affected the airflow field and the motion of the ratooning rice grains. Since numerical simulation could shorten the research period, and simulate and analyze the motion trail of the ratooning rice grains, the gas-solid two-phase flow simulation with different structural parameters of the mixing cavity was carried out.

Figure 5 Meshing of the mixing cavity

The calculation domain was subjected to meshing, and the total number of meshes was 98 576. Skewness was used as an index for checking the quality of the meshes. The obtained results showed that the skewness was greater than 0.7, indicating the good quality of the meshes. After detecting irrelevancy in the meshes, the analysis of the simulation was repeated three times by increasing the number of nodes by 1.5, 2.0, and 3.0 times, respectively. The results showed that the error in the calculation could be controlled within 5% with the mesh refinement. The results were not sensitive to the number of meshes, which met the requirements for the irrelevance detection.

4.1 Mathematical model of the flow field

The volume fraction of ratooning rice grains in the mixing cavity was large. It had a significant influence on the flow field, and hence it was taken into account in the CFD-DEM coupling. Therefore, the Eulerian model was selected in this study, which is solved in a multiphase flow framework and applicable to the flow field law inside the mixing cavity.

CFD was used for numerical simulation of the flow field inside the mixing cavity. There were backflow and jet flow in the mixing cavity due to its special structure, and the airflow was turbulent. Hence, the standard k-ε model was applied, which is highly robust and capable to precisely capture the data variation at each point in a flow field[21-23]. In the CFD-DEM coupling simulation module, the particle-fluid interaction force acting on particles include two major forces: the drag force, and the pressure gradient force. In addition, lift forces such as Saffman force and Magnus force are also considered[24]. In the airflow field of the mixing cavity, the distribution of the airflow field and the moving characteristics of the rationing rice grains could be clarified by means of the gas-solid coupling simulation analysis[25]. In the Eulerian model, the continuity and momentum equations of the gas-phase under the two-phase flow are given below[26]:

$$\frac{\partial(\varepsilon\rho)}{\partial t}+\nabla(\rho\varepsilon v)=0 \tag{13}$$

where, ρ is the gas density, kg/m^3; t is time, s; v is the gas velocity, m/s; ε is gas volume fraction phase; ∇ is the Hamiltonian differential operator.

$$\frac{\partial(\varepsilon\rho v)}{\partial t}+\nabla(\rho\varepsilon v^2)=-\nabla P+\nabla(\mu\varepsilon\nabla v)+\rho\varepsilon g-s \tag{14}$$

where, P is the fluid pressure, Pa; μ is aerodynamic viscosity, Pa s; s is the source term, kg/m^2 s^2.

Reynolds number Re can be used as follows to characterize the gas flow in the mixing cavity:

$$Re=\frac{\rho v D}{\mu} \tag{15}$$

The gas inlet diameter D was 180 mm, gas velocity was greater than 15 m/s. Accordingly, the gas flow in the mixing cavity was turbulent.

4.2 Contact model

DEM was used to describe the collision process between grains, which was divided into hard-sphere model and soft-sphere model according to different collision modes. In the soft-sphere model, overlapping and a certain collision time between grains were allowed. It was assumed in the soft-sphere model that the grain collision was a process developed with time, and its physical model was equivalent to a set of springs, dampers, and sliding blocks, where the elastic action, buffer action, friction, slip, rolling, and locking were taken into account during the solid grain collision[27]. Accordingly, the soft-sphere model was more applicable for solving the dense phase flow with relatively continuous interaction between grains, which at present is the best choice for full-scale simulation of the dense phase flow.

No force was introduced to the coupler, which was only used to confirm the pairing relationship between the colliding grains. In the tangential direction, when the tangential force exceeded the yield value, the two grains slid under the action of the normal and friction forces, which was realized by the slider[28]. Compared to the actual situation, the soft-sphere model and Hertz-Mindlin non-slip contact model were selected in this study, which is shown in Figure 6.

4.3 Ratooning rice grain model

In the discrete element software, the method of the original grain aggregate was used for simulating the real material[29,30], and the ratooning rice grain model was formed in EDEM by the method of multi-sphere combination and superposition[31-33], as shown in Figure 7.

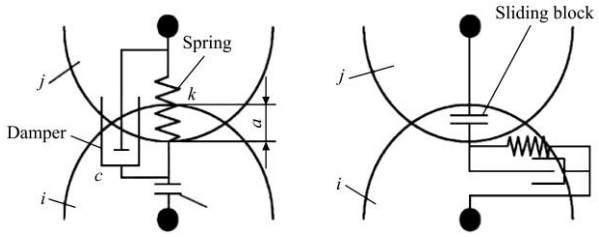

a. Normal contact model b. Tangential contact model

Figure 6 Schematic diagram of the soft-sphere model

a. Ratooning rice grain model b. Ratooning rice grain

Figure 7 Ratooning rice grain

4.4 Flow field parameters

Different sectional parameters of the mixing cavity had a great influence on the gas flown in the mixing cavity, affecting the motion of ratooning rice grains. Three parameters of the mixing cavity are listed in Table 2. After obtaining the optimal sectional parameters of the mixing cavity, the influence of the length of the contraction section in the mixing cavity on the motion of ratooning rice grains was studied. In the simulation, three different lengths of the contraction section in the mixing cavity were examined through the preliminary single factor test, which was 180 mm, 220 mm and 260 mm. In each case, the airflow velocity was set to be 20 m/s at the inlet.

Table 2 Characteristic parameters of the mixing cavity

Parameter	Height of the contraction section h/mm	Contraction angle θ/(°)	Length of the contraction section L/mm
Type I	90	135	180
Type II	120	145.9	180
Type III	150	160.6	180

4.5 Simulation of the conveying process

The EDEM-Fluent coupling process is a transient bidirectional data transferring process. In this study, the step-wise information of the flow field was first calculated by Fluent, and then EDEM has initiated for the same time iteration. The position, motion and velocity of the ratooning rice grains were transmitted to Fluent via the coupling interface. The interaction between the ratooning rice grains and airflow was calculated. The effect of the airflow on the ratooning rice grains was transmitted to EDEM via the interface for influencing the motion of the ratooning rice grains. The airflow acted on the fluid by means of the momentum source phase to perform gradual loop iteration, thereby realizing the transient simulation of the whole process. In this study, the boundary condition to the inlet velocity in the flow field was 20 m/s. The time step of EDEM was 1×10^{-6} s and that of Fluent was 1×10^{-3} s, which was 1000 times higher than the former. For Fluent, the number of steps was set to be 5000. The simulation time was 5 s. Each time step was subjected to not more than 20 iterations.

In order to study the airflow field in the mixing cavity and the motion of the ratooning rice grains, the changes in the flow field, coupling field and grain field under different parameters were simulated by CFD-DEM, so as to obtain the optimal structure parameters of the mixing cavity.

5 Analysis of simulation results

5.1 Model verification

Different types of mixing cavity parameters only affect the motion state of rice, choose one type of mixing cavity at will for bench test to verify the feasibility of CFD-DEM, a test performance was built as shown in Figure 15. In this test, the inlet wind velocity was set as 20 m/s and the speed of the screw conveyor was set as 1000 r/min. When the wind velocity and the feeding rate of ratooning rice grains were stable, the weight of the ratooning rice grains collected at the outlet was recorded every 5 s. Productivity of the screw conveyor Q can be expressed as follows:

$$Q=\frac{\pi}{24}\left[(S-2\lambda)^2-d^2\right]\psi tn\gamma C\times10^{-10} \tag{16}$$

where, λ is the clearance between the conveyor blade and shell, mm; n is conveyor speed, r/min; ψ is the fullness coefficient of conveying grains; γ is the mass per unit volume of ratooning rice, kg/m^3; C is the inclined conveying coefficient of the conveyor.

Screw conveyor power consumption N can be obtained as follows:

$$\begin{aligned}N&=Qg(LW_0+H)\eta\times10^{-3}\\&=Q(LW_0+H)\eta/102\end{aligned} \tag{17}$$

where, L is the horizontal projection length of the conveyor, m; Q is screw conveyor productivity, kg; H is the lifting height of ratooning rice grains, m; W_0 is the resistance coefficient of the shell movement of ratooning rice grains; η is correction coefficient.

Table 3 Inclined conveying coefficient C

Angle of inclination	0 °	30 °	40 °	60 °	70 °	90 °
Conveying coefficient	1	0.82	0.76	0.64	0.58	0.46

Table 4 Correction coefficient

Angle of inclination	20 °	25 °	30 °	35 °	40 °	45 °
Correction coefficient	1	1.05	1.13	1.20	1.32	1.40

The performance test results were compared with the simulation results. The mass of the ratooning rice grains was calculated in every 5 s. The results are shown in Figure 8. The simulation results were obtained under ideal environmental conditions, only rice grains move in the screw conveyor of the combined harvester, but in the actual environment, lighter impurities such as rice empty shell and straw debris will be mixed in the screw conveyor of the combined harvester. In addition, the inner surface of the screw conveyor device is rough, and the moving speed of rice particles is lower than that in the ideal environment. So, the simulation value was slightly higher. Although the two curves were not exactly same, their difference was so small that the simulated results could be considered to be consistent with experiments.

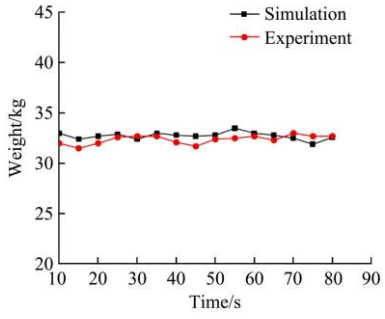

Figure 8 Comparison between performance test results and simulation results

The airflow field and distribution of grains in the mixing cavity are shown in Figure 9. It can be observed that the airflow velocity increased rapidly at the contraction section and gradually decreased after leaving this section. The pressure at the air inlet was large, then decreased significantly, and finally remained constant. In

addition, in order to observe the moving trajectory of rice grain, five representative trajectory lines are selected in the rice flow for observation, as shown in Figure 9c. The velocity of ratooning rice grains increased sharply after they entered the mixing cavity and undertaken the action of airflow, the characteristics of gas-solid two-phase flow were consistent with the actual situation. As a result, it is feasible to use CFD-DEM coupling to optimize the conveying device of ratooning rice.

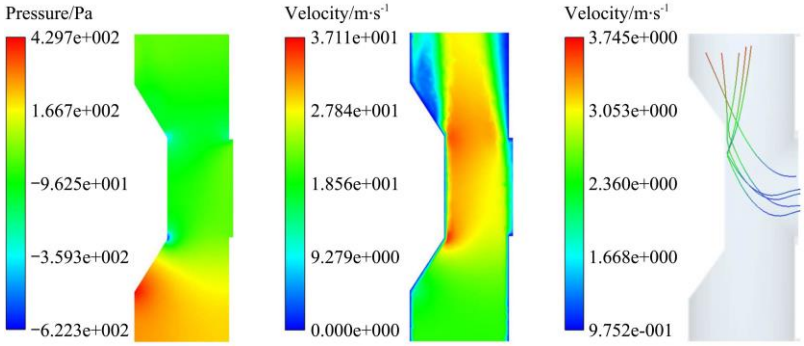

a. Pressure distribution b. Air velocity vector c. Grain location

Figure 9 Flow field and grain distribution in the mixing cavity when the wind velocity was 20 m/s and the speed of the horizontal screw conveyor was 1000 r/min

5.2 Influence of cross-sectional height of contraction section on grain motion

The conveyor connection part is the part that encounters clogging most easily. As shown in Figure 10, the pressure in the connection part increased greatly because of the stacking and compactness of the grain, which stopped the machine, damaged the grain, and seriously affected the harvesting quality. The mixing cavity was added to mix up the air flow and grains uniformly, so as to achieve continuous conveying of the grains. The partial fluid pressure and the grain velocity were affected by the cross-sectional height h of the contraction section of the mixing cavity. The distribution of the flow velocity in the mixing cavity was affected by the length L of the contraction section.

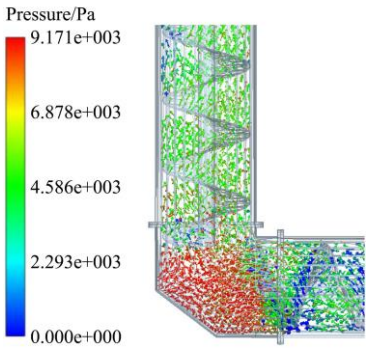

Figure 10 The conveyer is clogged up

In order to further analyze the influence of the cross-sectional height of the mixing cavity on the motion of a grain, the horizontal displacement (X=0 means the horizontal axis at the rice inlet) of the grain and its occurrence time (t=0 s means the time for air entering into the mixing cavity) at the outlet were analyzed. The analysis results are shown in Figure 11. It was found that when cross-section of type III was adopted, the grain processing rate was reduced. This is because of the fact that due to the low airflow speed and weak grain-airflow interaction, most grains would fall down first and then rise up after entering the mixing cavity. Meanwhile, due to the wide range of the X-axis, good diffusion could be realized. When type I mixing cavity was used, the grain processing rate increased due to the small sectional area of the contraction section and the high airflow velocity. The small range of the X-axis and the poor diffusion would affect the delivery of the grains into the vertical conveying pipe, thus lowering the delivery efficiency. When type II mixing cavity was applied, both airflow velocity and grain processing rate were relatively high. In addition, because of the wide range of the X-axis and the good diffusion effect, the delivery efficiency was high.

As shown in Figure 11, the grain uniformity could be clearly observed based on the occurrence time interval (Δt) of two consecutive grains. It was obvious that more grains were conveyed in a small agglomerate form when type I mixing cavity was adopted. The time interval (Δt) was the longest and the minimum grains were conveyed when type III mixing cavity was used. The grain discharging rate was relatively uniform when type II mixing cavity was applied.

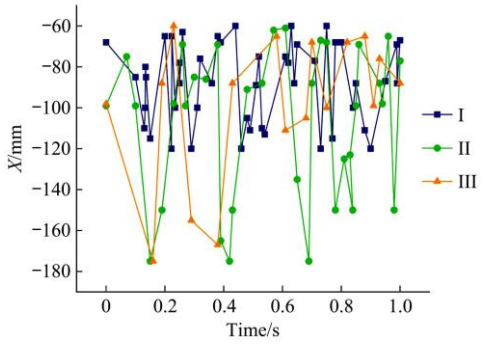

Figure 11 Time-position scatter plot of particle occurrence

As shown in Figure 12, the influence of different cross sectional sizes of the mixing cavity on the pressure and velocity of the airflow, and the grain motion was analyzed by assuming L = 180 mm and air inlet velocity = 20 m/s. It could be seen from the results that the pressure and velocity of the airflow were greatly affected by the cross-sectional height. When the air passed through the contraction section, the velocity was rapidly increased and the pressure was quickly minimized, generating a negative pressure lower than the atmospheric pressure. Later, the pressure was recovered and the velocity was decreased to a stable value. Among three cross-sectional sizes of the mixing cavity, the airflow velocity and the negative pressure of the cross-section of type I were the highest. Under the effect of the high-speed airflow, the grains were conveyed in the upward direction rapidly. However, the pressure loss and the low-speed airflow zone were the largest. The airflow velocity and the negative pressure of the cross-section of type III were the lowest. The grains were blown in the upward direction under the effect of the airflow. At the same time, the pressure loss and the low-speed airflow zone of the cross-section of

type III were the smallest. Due to the cross-sectional structure of type III, the grain-fluid interaction force was not large and the negative pressure was the lowest, weakening the suction of the grains and causing the backflow phenomenon. In the contraction section of type II, the velocity was maximized and the gradient pressure was varied rationally, thus causing a small loss. The pressure in the contraction section was lower than the atmospheric pressure, which could promote the suction of the grains. Therefore, the grains were evenly dispersed and delivered to the upward vertical conveying pipe under the effect of the airflow.

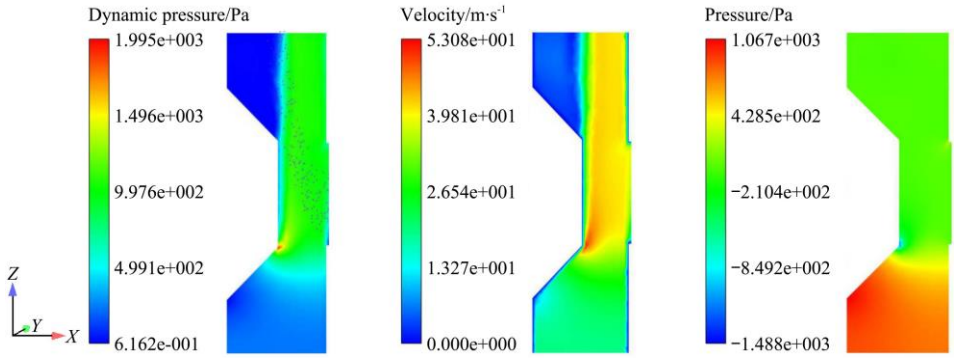

a. Cross-sectional height of 90 mm

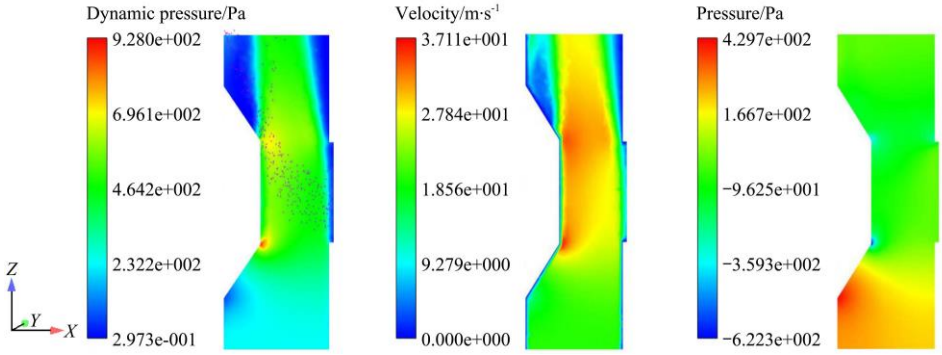

b. Cross-sectional height of 120 mm

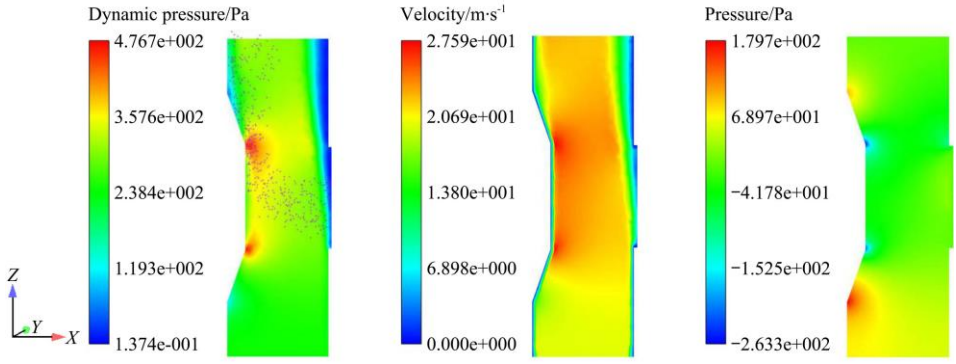

c. Cross-sectional height of 150 mm

Figure 12 Influences of different cross-sectional heights of contraction section on pressure, velocity, and grain motion

5.3 Influence of the length of contraction section on the grain motion

The fluid pressure, the velocity of the airflow and the motion of the grains under different lengths of the contraction section are shown in Figure 13. Under the initial conditions, the air inlet velocity was 20 m/s, the height of the contraction section was 120 mm and the rotating speed of the screw conveyor was 1000/min. The airflow field in the mixing cavity under all three lengths of the contraction section was basically the same. The airflow velocity was maximized in the contraction section and then it was gradually reduced.

The influence of the length of the contraction section on the airflow field and grain motion can be reflected by the motion trail of the grains. It was shown that in the initial stage, the grain was pushed into the mixing cavity at a slow speed by the horizontal screw conveyor. Then, the grain velocity was obviously increased under the action of the airflow pressure. When the length of the contraction section was 260 mm, the airflow velocity in the section was maximized and the high-speed airflow zone became larger. Basically, there was no low-speed airflow zone (the blue zone as shown in Figure 13c) and all the grains were uniformly distributed in the high-speed airflow zone. Then, with decreasing length of the contraction section, the high-speed airflow zone was reduced and the low-speed airflow zone (the blue zone as shown in Figure 13) was increased. The collision point of the grain and the contraction section was moved upward, causing some grains to move from the high-speed airflow zone to the low-speed airflow zone.

In order to quantify the influence of the contraction section

length on the airflow field and grain motion, a numerical simulation method was adopted, based on which the grain velocity and the force on the grain were extracted for creating a line chart as shown in Figure 14. The force on the grain along the direction of the pipe (*Z*-direction) was mainly the drag force. The velocity of the grain was relatively large along the *Z*-direction and small along the vertical direction (*X*-direction). With decreasing length of the contraction section, the collision rate of the grain and the contraction section was reduced and the joint force, as well as the *X*-direction force, were increased.

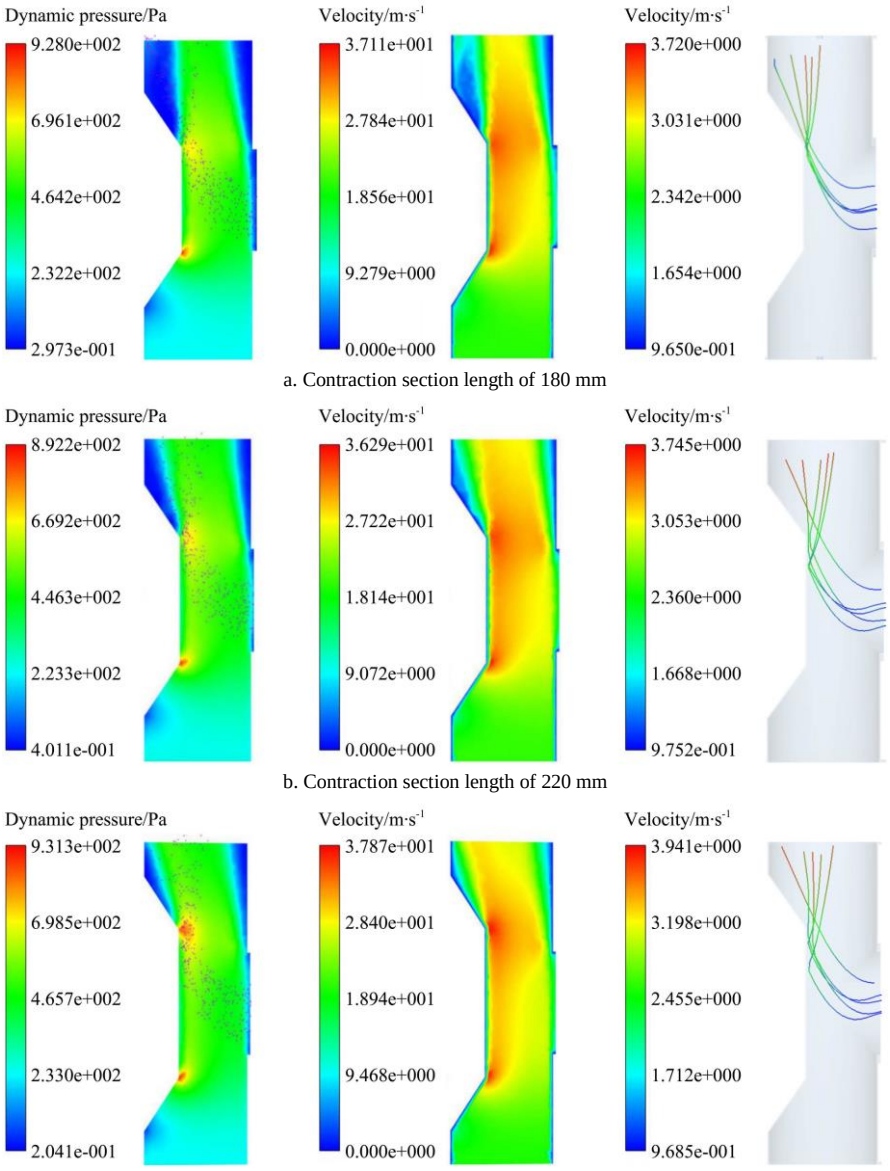

a. Contraction section length of 180 mm

b. Contraction section length of 220 mm

c. Contraction section length of 260 mm

Figure 13 Airflow field and grain distribution in the mixing cavity under the airflow velocity of 20 m/s and the rotating speed of the horizontal screw conveyor of 1000 r/min

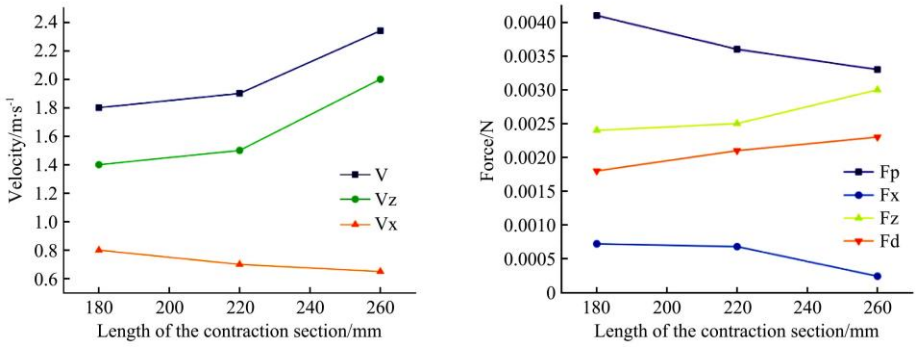

a. Velocity line chart

b. Line chart of the force on the grain

Figure 14 Mean forces and velocities acting on grain for different lengths of the contraction section

The grain stayed in the high-speed airflow zone for a shorter time, causing the ratooning rice to move directly from the high-speed airflow zone to the low-speed airflow zone. At the same time, the force and velocity along the Z direction were

reduced rapidly. When the length of the contraction section was 260 mm, the airflow velocity in the section was maximized, while the grain stayed in the high-speed airflow zone for the longest time and the largest drag force was achieved.

6 Performance text

The conveying performance of the grain unloading device is directly affected by the airflow velocity in the mixing cavity. It can be controlled by adjusting the rotating speed of the frequency conversion fan. A preliminary test was conducted. The obtained result showed that the grain could not be conveyed in time when the airflow velocity was relatively small. However, although the conveying performance could be improved by increasing the airflow velocity, the grain velocity at the outlet was too large, thus leading to the grain scattering. In addition, the normal stacking would be affected if the output ratooning rice stack were blown by the airflow.

Within a certain range, the conveyed quantity increased with increasing grain filling coefficient in the horizontal screw conveyor. However, when the filling coefficient was more than 0.5, the grain motion in the horizontal screw conveyor became unstable, thus resulting in grain rolling, moving around the axis, and mutual extruding. The power consumption in conveying was greatly increased and clogging took place.

In accordance with the Agricultural Machinery Design Manual[14], it can be confirmed that the fan speed is 2500-3000 r/min, the grain filling coefficient in the horizontal screw conveyor is 0.25-0.45 and the rotating speed of the horizontal screw conveyor is 1000- 1500 r/min.

6.1 Test materials and devices

As shown in Figure15, the grain of Meixiangzhan-2 (The water content of rice grain is 37.68%, and the 1000 grain weight is 21.85 g), the frequency conversion fan made by Hon&Guan and the WAAAX film pressure sensor (diameter: 18 mm, measuring range: 200 N, sensitivity: 0.5 N) were used to conduct the test. The AS-H5 high-precision anemometer made by Aicevoos was used to measure the airflow velocity. The filling coefficient is the ratio of the stacking cross-sectional area of rice grains to the cross-sectional area of the screw conveyor during the transportation of rice grains. Changing the elongation of the cover plate above the screw conveyor to adjust the stacking cross-sectional area of rice accumulation, so as to change the filling coefficient. The performance test was conducted in the Zengcheng Teaching and Research Bases, South China Agricultural University.

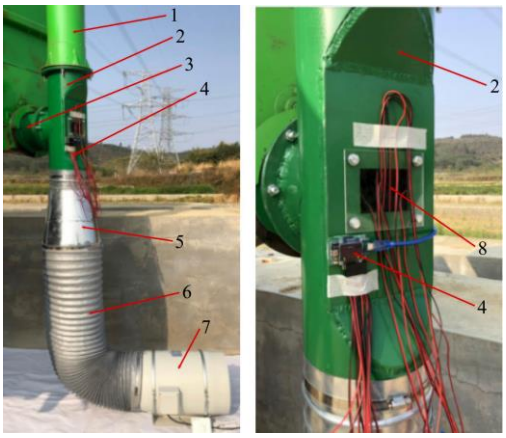

1. Vertical conveying pipe 2. Mixing cavity 3. Horizontal screw conveyor 4. Film pressure sensor 5. Reducer pipe 6. Air pipe 7. Frequency conversion fan 8. Viewing port

Figure 15 Performance test

6.2 Test design and method

The factors which could obviously affect the conveying performance, including the fan speed, filling coefficient, and rotating speed of the horizontal screw conveyor, were selected to conduct the three-factor quadratic regression orthogonal rotational combination test.

Table 5 Coding of factors and levels

Code	Fan speed /r·min^{-1}	Filling coefficient	Rotating speed of horizontal screw conveyor/r·min^{-1}
−1.682	2500	0.25	1000
−1	2601	0.29	1101
0	2750	0.35	1250
1	2899	0.41	1399
1.682	3000	0.45	1500

The evaluation was conducted based on the optimum outlet flow index, damage rate, and optimum pressure index of the mixing cavity. Each group of the test was repeated three times to obtain the average value.

Table 6 Test design and result

No.	Factor			Result		
	X_1	X_2	X_3	Y_1/%	Y_2/%	Y_3/%
1	−1	−1	−1	44.9	3.8	65
2	1	−1	−1	45.7	6.8	18
3	−1	1	−1	44.6	2.8	79
4	1	1	−1	45.6	3.2	56
5	−1	−1	1	44.5	6.5	44
6	1	−1	1	45.8	7.2	12
7	−1	1	1	43.6	4.7	81
8	1	1	1	44.9	4.9	53
9	−1.682	0	0	44.0	2.5	94
10	1.682	0	0	45.1	8.3	15
11	0	−1.682	0	47.1	3.8	19
12	0	1.682	0	45.2	2.1	75
13	0	0	−1.682	46.1	2.2	56
14	0	0	1.682	44.6	8.7	20
15	0	0	0	46.7	2.7	38
16	0	0	0	46.3	2.9	44
17	0	0	0	47.1	1.5	43
18	0	0	0	46.7	2.5	40
19	0	0	0	47.3	1.6	38
20	0	0	0	46.7	3.4	32
21	0	0	0	46.6	3.9	29
22	0	0	0	46.8	2.6	37
23	0	0	0	47.0	2.8	32

The optimum outlet flow index and pressure index of the mixing cavity were expressed in percentage values and referred to the variation range compared to the situation before optimization. The damage rate was worked out by measuring the quantity of the damaged grains out of 200 g grains. The damaged grains were weighed by the MH3000C electronic scale with accuracy of 1%.

The level codes of the test factors are shown in Table 5, and the design of the test and obtained results are summarized in Table 6. The fan speed, filling coefficient and rotating speed of the horizontal screw conveyor are separately expressed as X_1, X_2, and X_3, respectively. Also, the optimum outlet flow index, damage rate, and optimum pressure index of the mixing cavity are separately expressed as Y_1, Y_2, and Y_3, respectively. In order to reduce contingency, the central point is taken as 9 in this experiment, a total of 23 groups of tests were carried out.

6.3 Mathematical model of regression and significance test

The multiple regression fitting of the test data was conducted by Design-Expert 8.0.6 software. Based on the regression

analysis of the test results, a regression equation in terms of the optimum outlet flow index Y_1, damage rate Y_2, and optimum pressure index of the mixing cavity Y_3 could be established.

6.3.1 Optimum outlet flow index Y_1

Based on the test results and multiple regression fitting of the test data, the following regression model was established for evaluating the influence of various factors on the optimum outlet flow index Y_1:

$$Y_1 = 46.81 + 0.46X_1 - 0.40X_2 - 0.33X_3 + 0.025X_1X_2 + 0.10X_1X_3 - 0.17X_2X_3 - 0.86X_1^2 - 0.30X_2^2 - 0.58X_3^2 \quad (18)$$

The significance test of the regression equation is listed in Table 7, where it can be seen that the model had a significant fitness degree (p<0.01). However, the p values of the interaction of the fan speed and filling coefficient (X_1X_2), the interaction of the fan speed and rotating speed of the horizontal screw conveyor (X_1X_3), and the interaction of the filling coefficient and rotating speed of the horizontal screw conveyor (X_2X_3) were over 0.1, indicating that the above items did not have a significant influence on the optimum outlet flow index. The P values of all other items show that the influence was significant, proving that the test factor did not simply have linear influence but also had a quadratic influence on the response value. The lack of fit was not significant (p=0.1788), indicating that the index was not greatly affected by other factors. The determination coefficient of the regression equation R^2 reached 0.94, proving that the value predicted by the regression equation was well fitted with the actual value. After removing the insignificant factors, the regression model took the following form:

$$Y_1 = 46.81 + 0.46X_1 - 0.40X_2 - 0.33X_3 - 0.86X_1^2 - 0.29X_2^2 - 0.58X_3^2 \quad (19)$$

For validating the coefficients of Equation (19), the factors were ranked as the fan speed, filling coefficient and rotating speed of the horizontal screw conveyor based on their influence degree on the optimum outlet flow index.

6.3.2 Damage rate Y_2

Based on the test results and multiple regression fitting of the test data, the following regression model was formed for evaluating the influence of various factors on the damage rate Y_2:

$$Y_2 = 2.65 + 1.03X_1 - 0.85X_2 + 1.29X_3 - 0.39X_1X_2 - 0.31X_1X_3 + 0.062X_2X_3 + 1.03X_1^2 + 0.16X_2^2 + 1.04X_3^2 \quad (20)$$

The significance test of the regression equation is shown in Table 7, where it can be seen that the model had a significant fitness degree (P<0.01). However, the P values of the interaction of the fan speed and filling coefficient (X_1X_2), the interaction of the fan speed and rotating speed of the horizontal screw conveyor (X_1X_3), the interaction of the filling coefficient and rotating speed of the horizontal screw conveyor (X_2X_3), and the second-order of the filling coefficient (X_2^2) were over 0.1, indicating that the above items did not have significant influence on the damage rate. The P values of all other items show that the influence was extremely significant or significant, proving that the related test factor did not simply have linear influence but also had quadratic influence on the response value. The lack of fit was not significant (p=0.0523), indicating that the index was not greatly affected by other factors. The determination coefficient of the regression equation R^2 reached 0.8454, proving that the value predicted by the regression equation was well fitted with the actual value. After removing the not significant factors, the regression model took the following form:

$$Y_2 = 2.75 + 1.03X_1 - 0.85X_2 + 1.29X_3 + 1.03X_1^2 + 1.04X_3^2 \quad (21)$$

For validating the coefficients of Equation (21), the factors were ranked as the rotating speed of the horizontal screw conveyor, fan speed, and filling coefficient based on their influence degree on the damage rate.

Table 7 Variance analysis of regression equation

Variance source	Optimum outlet flow index				Damage rate				Optimum pressure index of the mixing cavity			
	Square sum	Degree of freedom	F	p	Square sum	Freedom degree	F	p	Square sum	Degree of freedom	F	p
Model	25.05	9	22.81	<0.0001**	83.18	9	7.9	0.0005**	10600.02	9	23.37	<0.0001**
X_1	2.86	1	23.44	0.0003**	14.46	1	12.36	0.0038**	5059.45	1	100.39	<0.0001**
X_2	2.13	1	17.47	0.0011**	9.78	1	8.36	0.0126*	3679.97	1	73.02	<0.0001**
X_3	1.50	1	12.27	0.0039**	22.76	1	19.46	0.0007**	574.08	1	11.39	0.0050**
X_1X_2	0.005	1	0.041	0.8427	1.20	1	1.03	0.3294	98.00	1	1.94	0.1866
X_1X_3	0.080	1	0.66	0.4327	0.78	1	0.67	0.4286	12.50	1	0.25	0.6268
X_2X_3	0.24	1	2.01	0.18	0.031	1	0.027	0.8727	84.50	1	1.68	0.2179
X_1^2	11.76	1	96.33	<0.0001**	16.73	1	14.3	0.0023**	778.75	1	15.45	0.0017**
X_2^2	1.38	1	11.29	0.0051**	0.41	1	0.35	0.5655	300.55	1	5.96	0.0297*
X_3^2	5.30	1	43.40	<0.0001**	17.31	1	14.80	0.0020**	21.65	1	0.43	0.5237
Residual	1.59	13			15.21	13			655.19	13		
Lack of fit	0.89	5	2.03	0.1788	10.55	5	3.62	0.0523	445.19	5	3.39	0.0612
Error	0.70	8			4.66	8			210.00	8		
Sum	26.64	22			98.38	22			11255.22	22		

Note: * significant (p<0.05) and ** extremely significant (p<0.01).

6.3.3 Optimum pressure index of the mixing cavity Y_3

Based on the test results and multiple regression fitting of the test data, the following regression model was established for evaluating the influence of various factors on the optimum pressure index of the mixing cavity Y_3:

$$Y_3 = 36.92 - 19.25X_1 + 16.42X_2 - 6.48X_3 + 3.50X_1X_2 + 1.25X_1X_3 + 3.25X_2X_3 + 7.00X_1^2 + 4.35X_2^2 + 1.17X_3^2 \quad (22)$$

The significance test of the regression equation is shown in Table 7, where it can be seen that the model had a significant fitness degree (p<0.01). However, the P values of the interaction of the fan speed and filling coefficient (X_1X_2), the interaction of the fan speed and rotating speed of the horizontal screw conveyor (X_1X_3), the interaction of the filling coefficient and rotating speed of the horizontal screw conveyor (X_2X_3), and the second-order of the rotating speed of the horizontal screw conveyor (X_3^2) were over 0.1, indicating that the above items did not have significant influence on the optimum pressure index of the mixing cavity. The P values of all other items show that the influence was

extremely significant or significant, proving that the related test factor did not simply have linear influence but also had quadratic influence on the response value. The lack of fit was not significant (p=0.0612), indicating that the index was not greatly affected by other factors. The determination coefficient of the regression equation R^2 reached 0.9418, proving that the value predicted by the regression equation was well fitted with the actual value. After removing the not significant factors, the regression model took the following form:

$$Y_3=37.62-19.25X_1+16.42X_2-6.48X_3+6.99X_1^2+4.34X_2^2 \quad (23)$$

For validating the coefficients of Equation (23), the factors were ranked as the fan speed, filling coefficient, and rotating speed of the horizontal screw conveyor based on their influence degree on the optimum pressure index of the mixing cavity.

6.4 Influence of various factors on optimum outlet flow index

The influence of the fan speed, filling coefficient, and rotating speed of the horizontal screw conveyor on the optimum outlet flow index could be observed by relying on the data processed by the Design-Expert 8.0.6 software. The corresponding response surface chart is shown in Figure 16. By fixing a factor randomly, the interaction influence of the left two factors on the optimum outlet flow index was analyzed relying on response surface chart.

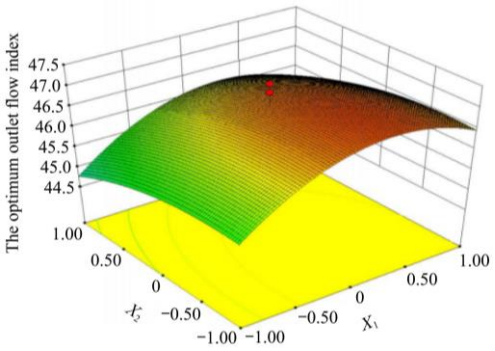

a. Interaction of fan speed and filling coefficient

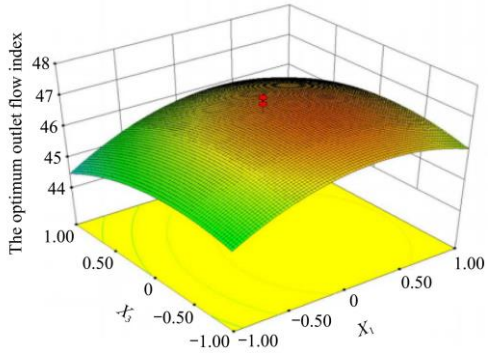

b. Interaction of fan speed and rotating speed of horizontal screw conveyor

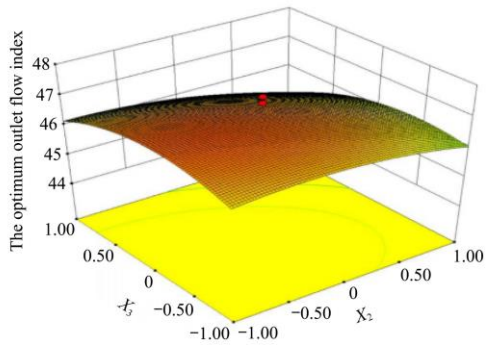

c. Interaction of filling coefficient and rotating speed of horizontal screw conveyor

Figure 16 Effects of interactive factors on the optimum outlet flow index

6.4.1 Interaction of the fan speed and filling coefficient

The response surface chart, revealing the influence of the fan speed and filling coefficient interaction on the optimum outlet flow index, is shown in Figure 16a against the rotating speed of 1250 r/min of the horizontal screw conveyor. Based on the chart, it was found that when the fan speed was fixed, the optimum outlet flow index increased first and then decreased with increasing filling coefficient. In addition, when the filling coefficient was fixed, the optimum outlet flow index increased first and then decreased with increasing fan speed.

6.4.2 Interaction of the fan speed and rotating speed of the horizontal screw conveyor

The response surface chart, revealing the influence of the interaction of the fan speed as well as the rotating speed of the horizontal screw conveyor on the optimum outlet flow index, is shown in Figure 16b against the filling coefficient of 0.35. It could be observed from the chart that when the fan speed was fixed, the optimum outlet flow index increased first and then decreased with the increasing rotating speed of the horizontal screw conveyor. Besides, when the rotating speed of the horizontal screw conveyor was fixed, the optimum outlet flow index increased first and then decreased with increasing fan speed.

6.4.3 Interaction of the filling coefficient and rotating speed of the horizontal screw conveyor

The response surface chart, revealing the influence of the interaction of the filling coefficient and rotating speed of the horizontal screw conveyor on the optimum outlet flow index, is shown in Figure 16c against the fan speed of 2750 r/min. It could be seen from the chart that when the filling coefficient was fixed, the optimum outlet flow index increased first and then decreased with an increase in the rotating speed of the horizontal screw conveyor. When the rotating speed of the horizontal screw conveyor was fixed, the optimum outlet flow index increased first and then decreased with an increase in the filling coefficient.

6.5 Optimal parameters

The optimal parameters could be obtained by setting the damage rate to be less than 2.5% and by maximizing the outlet flow index and the pressure index of the mixing cavity. When the rotating speed of the horizontal sector conveyor, fan speed and filling coefficient were 1173 r/min, 2706 r/min and 0.41, respectively, the optimum outlet flow index and optimum pressure index of the mixing cavity were over 45.9% and 68.1%, respectively, and the damage rate was less than 1.3%.

In order to validate the optimum results, the test was repeated for 3 times and the obtained results were compared with those of the non-improved grain unloading system. When the optimal parameters were used, the practical value was found close to the theoretical value. Also, all of the optimum outlet flow index, optimum pressure index of the mixing cavity, and damage rate were better than those of the original grain unloading system, thus proving the obvious effects of optimization.

7 Discussion

The conveying performance test is carried out by using the Meixiangzhan-2 grains as the test material. It was found from the test results that the proposed grain unloading and conveying device could effectively improve the outlet flow and reduce the grain damage rate. This is mainly because by relying on the airflow device, the grain flow and the high-speed airflow collide in the mixing cavity, thus dispersing the grain, improving the grain fluidity, and avoiding the clogging problem. In comparison to the

screw conveying system, the improved system could allow the grains to take a shorter path and a higher speed. Additionally, the designed mixing cavity accelerated the motion of the grains in the pipe of the mixing cavity and improved the outlet flow. The air-solid mixing cavity was installed at the joint of the horizontal and vertical conveying pipes by replacing the traditional double-screw connection and effectively reducing the grain damage rate.

Due to the high water content and poor fluidity of the grain used in the test, it was difficult to convey it by the traditional double-screw unloading and conveying device. The test was conducted only on the grains with the same water content. Also, the influence of different water content on the outlet flow of the unloading and conveying device, and grain damage rate were not analyzed.

8 Conclusions

In this study, aiming at the problem that the unloading device of ratooning rice harvester is easy to be blocked in South China, an air flow ratooning rice conveying device was developed. The CFD-DEM coupling method was applied for simulating and analyzing the motion and flow field of the grain in the conveying system under different conditions. The influences of the cross-sectional height of the mixing cavity, height of the contraction section, airflow velocity, and other parameters on the conveying of the ratooning rice were analyzed. The conclusion of the work is as follows:

1) The clogging problem of the conveying device of the ratooning rice harvester is solved. For this, a pneumatic conveying device was designed and the mechanical pneumatic conveying technology was combined with it to mitigate the clogging.

2) The causes of clogging in the traditional conveying device are analyzed. Owing to the special structure of the mixing cavity designed based on the Venturi principle, the grain could pass through the mixing cavity uniformly, orderly, and rapidly.

3) The influence of the cross-sectional height of the contraction section on the airflow field and the motion of the grain are analyzed. As per the obtained results, when the cross-sectional size is too small, the grain flow is affected and the dispersity, as well as the conveying efficiency, are decreased. On the other hand, when the cross-sectional size is too large, the effect of the negative pressure is not obvious and it is difficult to convey the grain upward through the vertical conveying pipe. When the cross-sectional height of the contraction section reaches 120 mm, good airflow field, high conveying dispersity of the grain and high conveying efficiency can be realized.

4) The drag force is obviously affected by the length of the contraction section. As seen in the results, when the length of the contraction section increases, the high-speed airflow zone also increases. While the length of the contraction section reaches 260 mm, the ratooning rice moves at a higher speed, thus promoting the grain to enter into the vertical conveying pipe rapidly.

5) The test factors of the fan speed, filling coefficient, and rotating speed of the horizontal screw conveyor are selected to conduct a three-factor quadratic regression orthogonal rotational combination test. It could be seen in the obtained results that when the fan speed, filling coefficient, and rotating speed of the horizontal sector conveyor are 2700 r/min, 0.41, and 1173 r/min, respectively, the optimum outlet flow index and optimum pressure index of the mixing cavity are over 45.9% and 68.1%, respectively, and the damage rate is less than 1.3%.

Acknowledgements

The authors would like to express their gratitude to EditSprings (https://www.editsprings.com/) for the expert linguistic services provided.

[References]

[1] Zhang M H, Wang Z M, Luo X W, Guo W J, Zang Y. Review of precision rice hill-drop drilling technology and machine for paddy. Int J Agric & Biol Eng, 2018; 11(3): 1–11.

[2] Zhang X L, Ma K, Wang H, Cui S J, Shi Y F. Effect of particle size on precision dosing of screw feeder. Transactions of the CSAE, 2014; 30(5): 19–27. (in Chinese)

[3] Wulan T Y, Wang C G, Qi S H, Yan J G, Wang J L. Test and analysis of performance of screw conveyor for rubbing and breaking corn straw. Transactions of the CSAE, 2015, 31(21): 51–59. (in Chinese)

[4] Tong Z B, Zheng B, Yang R Y. CFD-DEM investigation of the dispersion mechanisms in commercial dry powder inhalers. Powder Technology, 2013; 240: 19–24.

[5] Fernández X R, Nirschl H. Simulation of particles and sediment behaviour in centrifugal field by coupling CFD and DEM. Chemical Engineering Science, 2013; 94: 7–19.

[6] Ren B, Zhong W Q, Chen Y, Chen X, Jin B S. CFD-DEM simulation of spouting of corn-shaped particles. Particuology, 2012; 10(5): 562–572.

[7] Chu K W, Chen J, Wang B, Yu A B, Vince A, Barnett G D, et al. Understand solids loading effects in a dense medium cyclone: effect of particle size by a CFD-DEM method. Powder Technology, 2017; 320: 594–609.

[8] Han D D, Zhang D X, Yang L. EDEM-CFD simulation and experiment of working performance of inside filling air-blowing seed metering device in maize. Transactions of the CSAE, 2017; 33(13): 23–31. (in Chinese)

[9] Ismail N I, Kuang S, Yu A. CFD-DEM study of particle-fluid flow and retention performance of sand screen. Powder Technology, 2021; 378: 410–420.

[10] Peng Z, Doroodchi E, Moghtaderi B. Heat transfer modelling in discrete element method (DEM)-based simulations of thermal processes: Theory and model development. Progress in Energy and Combustion Science, 2020; 79: 100847. doi: 10.1016/j.pecs.2020.100847.

[11] Ge W, Wang L, Xu J, Chen F G, Zhou G Z, Lu L Q, et al. Discrete simulation of granular and particle-fluid flows: From fundamental study to engineering application. Reviews in Chemical Engineering, 2017; 33(6): 551–623.

[12] Li H C, Li Y M, Tang Z, Xu L Z, Zhao Z. Numerical simulation and analysis of vibration screening based on EDEM. Transactions of the CSAE, 2011; 27(5): 117–121. (in Chinese)

[13] Xu L Z, Li Y M. Critical speed of impact damage on a rice kernel. Transactions of the CSAM, 2009; 40(8): 54–57. (in Chinese)

[14] Agricultural Machinery Design Manual. Beijing: China Agricultural Science and Technology Press, November 2007.

[15] Li H T, Wan X Y, Xu Y, Jiang Y J, Liao Q X. Clearance adaptive adjusting mechanism for header screw conveyor of rape combine harvester. Transactions of the CSAM, 2017; 48(11): 115–122. (in Chinese)

[16] Tian R G, Lin J T, Wang H L, Ye T, Liang Y C, Bi J F. Study and design of conveying and cleaning system of corn harvester. Journal of Agricultural Mechanization Research, 2012; 34(6): 93–96. (in Chinese)

[17] Gao L X, Du X, Zhang W, Liu M G, Liu X, Yang J. Double-roller peanut sheller with pneumatic circulating. Transactions of the CSAM, 2011; 42(10): 68–73. (in Chinese)

[18] Zuo X J, Wu G W, Fu W Q, Li L W, Wei X L, Zhao C J. Design and experiment on air-blast rice side deep precision fertilization device. Transactions of the CSAE, 2016; 32(3): 14–21. (in Chinese)

[19] Wang J F, Gao G B, Weng W X, Wang J W, Yan D W, Chen B W. Design and experiment of key components of side deep fertilization device for paddy field. Transactions of the CSAM, 2018; 49(6): 92–104. (in Chinese)

[20] Akhshik S, Behzad M, Rajabi M. CFD-DEM approach to investigate the effect of drill pipe rotation on cuttings transport behavior. Journal of Petroleum Science and Engineering, 2015; 127: 229–244.

[21] Zhao Z, Li Y M, Liang Z W, Gong Z Q. DEM simulation and physical testing of rice seed impact against a grain loss sensor. Biosystems Engineering, 2013; 116: 410–419.

[22] Liu H X, Guo L F, Fu L L, Tang S F. Study on multi-size seed-metering device for vertical plate soybean precision planter. Int J Agric & Biol Eng, 2015; 8(1): 1–8.

[23] Dai F, Song X F, Guo W J, Zhao W Y, Zhang F W, Zhang S L. Simulation and test on separating cleaning process of flax threshing material based on gas-solid coupling theory. Int J Agric & Biol Eng, 2020; 13(1): 73–81.

[24] Gao X J, Zhou Z Y, Xu Y, Cui T. Numerical simulation of particle motion characteristics in quantitative seed feeding system. Powder Technology, Elsevier BV, 2020; pp.643–658. doi: 10.1016/j.powtec.2020.04.021.

[25] Lei X L, Liao Y T, Wang L, Wang D, Yao L, Liao Q X. Simulation of gas-solid two-phase flow and parameter optimization of pressurized tube of air-assisted centralized metering device for rapeseed and wheat. Transactions of the CSAE, 2017; 33(19): 67–75. (in Chinese)

[26] Yuan J B, Wu C Y, Li H, Qi X D, Xiao X X, Shi X X. Movement rules and screening characteristics of rice-threshed mixture separation through a cylinder sieve. Computers and Electronics in Agriculture, 2018; 154: 320–329.

[27] Mueller C R, Holland D J, Third J R, Sederman A J, Dennis J S, Gladden L F. Multi-scale magnetic resonance measurements and validation of Discrete Element Model simulations. Particuology, 2011; 9(4): 330–341.

[28] Gao X J, Xu Y, Yang L, Zhang D X, Li Y H, Cui T. Simulation and experiment of uniformity of venturi feeding tube based on DEM-CFD coupling. Transactions of the CSAM, 2018; 49(S1): 92–100. (in Chinese)

[29] Shi L R, Wu J M, Sun W, Zhang F W, Sun B G, Liu Q W, et al. Simulation test for metering process of horizontal disc precision metering device based on discrete element method. Transactions of the CSAE, 2014; 30(8): 40–48. (in Chinese)

[30] Yu Y J, Zhou H L, Fu H, Wu X C, Yu J Q. Modeling method of corn ears based on particles agglomerate. Transactions of the CSAE, 2012; 28(8): 167–174. (in Chinese)

[31] Dai F, Song X F, Zhao W Y, Han Z S, Zhang F W, Zhang S L. Motion simulation and test on threshed grains in tapered threshing and transmission device for plot wheat breeding based on CFD-DEM. Int J Agric & Biol Eng, 2019; 12(1): 66–73.

[32] Li H C, Li Y M, Gao F, Zhao Z, Xu L Z. CFD-DEM simulation of material motion in air-and-screen cleaning device. Computers and Electronics in Agriculture, 2012; 88(6): 111–119.

[33] Jiang E C, Sun Z F, Pan Z Y, Wang L J. Numerical simulation based on CFD-DEM and experiment of grain moving laws in inertia separation chamber. Transactions of the CSAM, 2014; 45(4): 117–122. (in Chinese)